Respiratory Research

RESEARCH

Open Access

# Aerosolized nicotine-free e-liquid base constituents exacerbates mitochondrial dysfunction and endothelial glycocalyx shedding via the AKT/GSK3β-mPTP pathway in lung injury models

Ziyu Dai[1,2], Bin Xie[1,2], Chen Jiang[1,2], Yun Peng[1,2], Jianing Lin[1,2], Qiong Chen[1,2] and Jingyi Sun[1,2*]

## Abstract

Smoking has been recognized as a risk factor of cancer, heart disease, stroke, diabetes, and lung diseases such as chronic obstructive pulmonary disease, and nicotine appears to be the responsible component of tobacco smoke that affects lung development. While nicotine-free electronic cigarettes (e-cigarettes) are often promoted as a safer alternative to traditional smoking, recent evidence suggests that they might pose significant health risks. This study investigates the effects of nicotine-free e-cigarette vapor (ECV) on lung tissue and endothelial function. A mouse model of ECV-induced lung injury and human pulmonary microvascular endothelial cells (HPMVECs) were utilized to evaluate the impact of ECV exposure on mitochondrial function, endothelial cell viability, and glycocalyx shedding. ECV exposure significantly damages lung tissue, characterized by alveolar enlargement, inflammation, and vascular remodeling, indicative of emphysematous changes. In vitro, HPMVECs exposed to nicotine-free e-cigarette extract (ECE) demonstrated dose-dependent increases in mitochondrial reactive oxygen species (ROS), mitochondrial membrane depolarization, mPTP opening, and reduced ATP production, leading to enhanced endothelial permeability and glycocalyx degradation. The inhibition of mPTP opening with Cyclosporin A (CsA) was found to mitigate the mitochondrial dysfunction and glycocalyx damage induced by ECE, indicating a protective role of mPTP inhibition in preserving endothelial integrity. The AKT/GSK3β signaling pathway was identified as a key regulator of these processes, with ECE exposure downregulating p-AKT and p-GSK3β, thereby promoting mPTP opening. Activation of AKT signaling partially reversed these effects, highlighting the potential of targeting the AKT/GSK3β-mPTP axis to mitigate the adverse effects of e-cigarette exposure on lung and endothelial function. These findings underscore the potential risks associated with nicotine-free e-cigarettes and suggest novel therapeutic targets for preventing lung injury progression.

**Keywords** Nicotine-free e-cigarette, Cytotoxicity, Mitochondrial dysfunction, Endothelial glycocalyx, AKT/GSK3β pathway, mPTP opening

*Correspondence:
Jingyi Sun
Jyi2024024@163.com
Full list of author information is available at the end of the article

## Introduction

Smoking is widely acknowledged as a significant risk factor for various serious health conditions, including cancer, heart disease, stroke, diabetes, and lung diseases such as chronic obstructive pulmonary disease (COPD) [1–4]. The harmful effects of smoking are largely attributed to nicotine, a key component in tobacco smoke, which plays a critical role in damaging lung tissue and impairing lung development [5]. Although nicotine exposure has been linked to the progression of several other systemic diseases, recent studies also indicate that nicotine-free products, such as certain electronic cigarettes (e-cigarettes), might pose potential risks to lung health [6].

E-cigarettes have been promoted as a less harmful alternative to traditional tobacco smoking [7]. However, emerging evidence suggests that e-cigarettes, including those that are nicotine-free, could still pose significant health risks [8]. Users who inhale e-cigarette vapor (ECV) are exposed to a complex mixture of chemicals and particulate matter, which induces oxidative stress, inflammation, and damage to lung tissue [8, 9]. Studies have shown that even without nicotine, e-cigarettes could induce inflammatory mediators release from COPD lung cells and potentially promote COPD occurrence and development [10]. Understanding the impact of nicotine-free e-cigarettes on lung health is crucial, particularly as their use continues to rise.

Mitochondrial dysfunction exerts a pivotal effect on chronic lung injury pathogenesis [11, 12]. The opening of the mitochondrial permeability transition pore (mPTP) is a crucial event resulting in the destruction of mitochondrial membrane potential, production of proapoptotic factors, and subsequent cell death [13, 14]. This mitochondrial damage contributes to endothelial dysfunction, a key feature in chronic lung injury, which impairs vascular homeostasis and promotes inflammation and tissue injury [15]. The endothelial glycocalyx, a protective microstructure layer on the vascular endothelium, is particularly vulnerable to oxidative stress and inflammation [16]. The vascular endothelial glycocalyx plays a vital role in endothelial function [17], since it is associated with microvascular reactivity, and regulates the crosstalk between the endothelium and blood components [18]. As recently reported, endothelial glycocalyx exerts a key effect on lung repair [19], and the endothelial glycocalyx impairment has been confirmed in chronic lung injury [20]. Therefore, damage to the endothelial glycocalyx might also exacerbate vascular permeability, inflammation, and the overall progression of chronic lung injury. Investigating the mechanisms underlying mPTP opening and endothelial glycocalyx injury is essential for developing targeted therapies to mitigate these effects.

The AKT/GSK3β pathway plays a crucial role in regulating cell survival, proliferation, and metabolism [21–23]. AKT activation results in the phosphorylation and repression of GSK3β, a kinase involved in numerous cellular processes [24]. Dysregulation of this pathway contributed to multiple diseases, including chronic lung injury [25]. As previously reported, the Akt-GSK3β-mPTP signaling could regulate mitochondrial dysfunction, thereby promoting glucose oxidative stress-induced apoptosis of odontoblasts [26]; it also modulates OPA1 cleavage linked to mitochondrial dysfunction, thereby improving the apoptosis of osteoblasts induced by oxidative stress [27]. Importantly, decreased Akt activation was observed with electronic cigarette vape exposure. Therefore, it has been hypothesized that nicotine-free e-cigarette smoke promotes mPTP opening via the AKT/GSK3β signaling, leading to worsened mitochondrial function and endothelial glycocalyx damage.

For validating the hypothesis, an animal model of nicotine-free e-cigarette vapor (ECV)-induced lung injury and human pulmonary microvascular endothelial cells (HPMVEC) exposed to different concentrations of e-cigarette extract (ECE) were used to evaluate mitochondrial function, endothelial cell viability, and the integrity of the endothelial glycocalyx. The findings are expected to elucidate the molecular mechanisms by which e-cigarette smoke exacerbates lung injury and identify potential targets for therapeutic intervention.

## Materials and methods

### Establishment of animal model

Sixteen-week-old male C57BL/6J mice were purchased from Hunan SJA Laboratory Animal Co. Ltd (Changsha, China) and used in this study. The mice were acclimatized for 2 weeks before the experiments. Mice were placed in a chamber and subjected to exposure to e-liquid (nicotine free, propylene glycol/vegetable glycerin is 50:50)-derived e-cigarette vapor (ECV), 5 days/week for 16 weeks, 4 times daily for 30 min, 5 days/week. The total matter concentration in the chamber at 130 mg/m$^3$. The vapor was generated by a commercial e-cigarette device (eVic Basic, JoyeTech, Shenzhen, China), equipped with a Tobeco Super Tank MINI with a 4 mL capacity and a 0.2 Ω coil made of Kanthal (iron/chromium/aluminum wire), which was set to a power output of 25 W, a voltage of 2.24 V, and a firing time of 5 s. This protocol was based on methods previously described [28].

### Preparation of bronchoalveolar lavage fluid (BALF)

After the final exposure, mice were euthanized with an overdose of isoflurane inhalation. The trachea was exposed, and a 20-gauge catheter was employed to cannulate. The lungs were subjected to 3 times lavage with 1 mL of sterile phosphate-buffered saline (PBS) each time, with the collected lavage fluid being pooled. The BALF was subjected to 10-min centrifugation at 300×*g* at 4 °C to pellet the cells. The collected supernatant was kept at −80 °C for subsequent analyses.

### Histological analysis and assessment

Cross sections of lung tissues were prepared and stained with haematoxylin and eosin (H&E) for histological analysis. Mean linear intercept analysis was performed on the H&E-stained lung sections, which were imaged using an Olympus slide scanner (VS120-SS, Olympus, Tokyo, Japan). This analysis was used to determine and quantify the extent of emphysema. Five randomly selected fields, at 20× magnification, from the distal regions of each lung section were analyzed. A 10×10 square grid was overlaid on each field, with each small square measuring 100 μm×100 μm. The grid was positioned to avoid regions containing vasculature and airways. The number of alveolar walls intersecting each horizontal grid line was counted. The mean linear intercept was then calculated by first subtracting the distance occupied by blood vessels and airways from the total length of each horizontal grid line, and then dividing the remaining distance by the total number of alveolar surface intersections counted. The average mean linear intercept across the five grids was calculated and used as the final mean linear intercept value for each lung sample [29].

### Immunohistochemistry

After being fixed and paraffin-embedded, lung tissue samples were sliced. Then, slices were deparaffinized and rehydrated before antigen retrieval. After eliminating endogenous peroxidase activity, slices were subjected to incubation with primary antibodies against α-SMA (14395-1-AP; Proteintech; Wuhan, China). Slices were washed, followed by incubation with HRP-labeled secondary antibodies. Next, DAB substrate was applied to visualize slices. The extent of staining was quantified using ImageJ software (version 1.47v; NIH, Bethesda, USA).

### Immunofluorescence staining (IF staining)

HPMVECs were fixed with 4% paraformaldehyde for 15 min at room temperature. Permeabilization was performed with 0.1% Triton X-100 for 10 min, followed by blocking with 5% BSA for 1 h at room temperature to reduce non-specific binding. After blocking, cells were incubated overnight at 4 °C with primary antibodies against CD31 (11265-1-AP, Proteintech), α-SMA (14395-1-AP, Proteintech), and Syndecan-1 (ab128936, Abcam, Cambridge, USA). Following primary antibody incubation, cells were washed three times with PBS, and then incubated with FITC- or Cy5-labeled secondary antibodies (Beyotime, Shanghai, China) for 1 h at room temperature. For tissue sections, a similar protocol was followed, using FITC- or Cy5-labeled secondary antibodies. Nuclei were counterstained with DAPI for 10 min. Fluorescence images were acquired using a inverted microscope (CKX53; Olympus, Tokyo, Japan) equipped with a fluorescence module from Shanghai Qibu Biotechnology Co., Ltd (BSW-CKX-UVBG-LED; Shanghai, China). The following settings were applied during image acquisition: Illumination Power: Optimized according to fluorophore-specific requirements; Exposure times: 200–300 ms for blue light, 500–700 ms for green light, 1–3 s for red light; Magnification: 100× (scale: 100 μm), 200× (scale: 50 μm), and 400× (scale: 20 μm) using appropriate objective lenses; Numerical Aperture: selected based on the objective lens used for each magnification to ensure high resolution. For image analysis, ImageJ software (version 1.47v; NIH) was used to assess protein localization and expression levels. Image quantification was performed by measuring fluorescence intensity and calculating the area of positive staining for each marker.

### Enzyme-linked immunosorbent assay (ELISA) and biochemistry analysis

Cell culture supernatants and lung tissue homogenates were collected to measure TNF-α (CSB-E04741m; CSB-E04740h; Cusabio, Wuhan, China), IL-6 (CSB-E04639m; CSB-E04639h; Cusabio), MMP-9 (CSB-E08007m; CSB-E08007h, Cusabio), MDA (BC0025; Solarbio, Beijing, China), SOD (A001-3-2; Nanjing Jiancheng Bioengineering Institute, Nanjing, China), and Syndecan-1 (ab273165; ab46506; Abcam) levels using commercial ELISA kits or biochemistry kits as per the protocols of the manufacturer. A microplate reader (BioTek, Winooski, USA) was applied to measure absorbance at the appropriate wavelength, and concentrations were calculated according to standard curves.

### Cell culture and treatment

Human pulmonary microvascular endothelial cells (HPMVEC) were procured from PromoCell (C-12281; St. Louis, USA) and cultivated in endothelial cell growth media containing 0.4% endothelial cell growth factor, 10 ng/mL recombinant human

epidermal growth factor, 90 μg/mL heparin, 1 μg/mL hydrocortisone, 1% antibiotics, and 5% fetal calf serum. Cells between passages 2 and 6 were used. Before treatment, cells were serum-starved with 1% fetal calf serum for 24 h. The e-cigarette extracts (ECE) were prepared as previously described [30]. The vapor from 0.8 mL nicotine-free e-liquid was bubbled in a Falcon tube containing 10 ml complete culture medium; the preparation is considered a 100% ECE. After sterile-filtered by 0.22 μm filter, ECE was diluted to final concentrations of 10%, 20%, and 30% with complete culture medium for treatment (L-ECE, M-ECE and H-ECE). Control cells received no ECE exposure. For mPTP block or AKT activation, HPMVECs received pre-treatment with 10 μM CsA (mPTP blocker) or 4 μg/mL SC79 (AKT activator) before exposure to 30% ECE for 24 h [31].

#### Immunoblotting

After lysing the cells, a BCA assay was employed to determine protein contents. Following electrophoresis by SDS-PAGE, equal amounts of proteins were electroblotted from the gel onto PVDF membranes. Membranes were subjected to blocking with 5% skim milk, followed by an overnight incubation at 4 °C with primary antibodies against p-AKT (Y011054, Affinity, Changzhou, China), AKT (Y409094, Affinity), p-GSK3β (Ser9; ab75814, Abcam), GSK3β (ab32391, Abcam), and GAPDH (60004-1-IG, Proteintech). Membranes were washed, followed by incubation with HRP-labeled secondary antibodies. An ECL detection system (Bio-Rad, Hercules, USA) was utilized to visualize, and densitometry was used to quantify protein bands.

#### Quantitative reverse transcription polymerase chain reaction (qRT-PCR)

The RNeasy Mini Kit (QIAGEN, Duesseldorf, Germany) was employed as per the protocols of the manufacturer to extract total RNA from target cells. A NanoDrop spectrophotometer (Thermo Fisher Scientific, Waltham, USA) was applied to assess RNA purity and concentration. The High-Capacity cDNA Reverse Transcription Kit (Applied Biosystems, Foster City, USA) was utilized to synthesize cDNA from 1 μg of total RNA. The Power SYBR Green PCR Master Mix (Applied Biosystems) on a StepOnePlus Real-Time PCR System (Applied Biosystems) was used to perform quantitative PCR. Specific primers (listed in Table S1) for TNF-αand IL-6 were used, with GAPDH serving as the internal reference. The $2^{-\Delta\Delta Ct}$ method was applied to calculate relative gene expression.

#### Determination of mitochondrial DNA release

HPMVECs were exposed to different treatments and then were divided into two equal parts. Resuspend the first part in 500 μL of DNA extraction buffer (Tiangen, Beijing, China). This resulting extract was used as a normalized control for the total amount of mtDNA. Resuspend the second part in 500 μL buffer composed of 25 mg/mL digitonin, 150 mM NaCl, and 50 mM HEPES (pH 7.4). Cell membranes were then permeabilized by incubation at room temperature for 10 min. Following this, the sample was centrifuged at 1000×*g* for 10 min to pellet intact cells. The supernatant containing the cytosol was carefully transferred to a new tube and then subjected to further centrifugation at 17,000×*g* for 10 min to remove any remaining cellular debris. The DNA present in the cytosolic fraction and whole-cell extracts was isolated using a DNA isolation kit from Tiangen. The mtDNA/nuclear DNA (nDNA) ratio was calculated to determine the mtDNA copy number. mtDNA was determined using primers for mitochondrial-specific genes ND1, COX1 and D-Loop. The nDNA was determined using primers for 18S. The mtDNA/nDNA ratio was calculated to determine the mtDNA copy number. The sequence of primers is listed in Table S1.

#### Mitochondrial reactive oxygen species (ROS) measurement

MitoSOX Red mitochondrial superoxide indicator (Invitrogen, Carlsbad, USA) was employed to assess mitochondrial ROS levels. HPMVEC were subjected to 10-min incubation at 37 °C away from light with 5 μM MitoSOX Red reagent. Subsequently, cells were rinsed thrice in PBS to eliminate excess dye. A fluorescence microscope (excitation wavelength: 510 nm; emission wavelength: 580 nm) was employed to measure fluorescence intensity. ImageJ software was applied to perform quantitative analysis of fluorescence images.

#### Mitochondrial membrane potential assessment

JC-1 dye (Invitrogen) was utilized to evaluate mitochondrial membrane potential. HPMVEC were subjected to 20-min incubation at 37 °C with 2 μM JC-1 dye. Subsequently, after two washings, cells were re-suspended in fresh media. A fluorescence microscope was used to measure fluorescence. Changes in mitochondrial membrane potential were assessed by calculating the ratio of red fluorescence (aggregates) to green fluorescence (monomers), with a decreased ratio indicating depolarization of the mitochondrial membrane.

### mPTP opening assay

A mitochondrial permeability transition pore assay kit (C2009S, Beyotime) was employed to detect mPTP opening. HPMVEC were loaded with a calcein-AM and $CoCl_2$ mixture as per the kit's instructions. A fluorescence microscope (excitation wavelength: 488 nm; emission wavelength: 505 nm) was used to observe fluorescence intensity. A decrease in calcein fluorescence indicated mPTP opening. The fluorescence intensity was normalized to control values to quantify the extent of mPTP opening.

### ATP level measurement

A CellTiter-Glo® One Solution Assay kit (Promega, Madison, USA) was employed to measure intracellular ATP levels. HPMVEC incubated with CellTiter-Glo® One Solution in 96 well for 2 min on shaker to induced cell lysis. A microplate reader was applied to measure luminescence after 10 min. ATP concentrations were determined by comparison with an ATP standard curve, with normalization to cell numbers.

### Endothelial permeability assay

A FITC-dextran leakage assay was employed to assess endothelial permeability. Confluent HPMVEC monolayers were cultured upon Transwell inserts with a 0.4 μm pore size (Corning Incorporated, Corning, USA). After various treatments, the top chamber of the Transwell insert was supplemented with 1 mg/mL FITC-dextran (Sigma-Aldrich, St. Louis, USA). After being incubated at 37 °C for 1 h at dark, 100 μL specimens were harvested from the lower chamber, and a microplate reader (excitation wavelength: 485 nm; emission wavelength: 530 nm) was utilized to measure the fluorescence intensity. The relative fluorescence intensity was normalized to the control group.

### Statistical analysis

GraphPad Prism version 8.0 (GraphPad Software, San Diego, USA) was applied to analyze data. The animal experiments were performed at least six times independently. The cell experiments were performed at least in triplicate independently. Data were presented in terms of mean ± standard deviation (SD). The Shapiro–Wilk test was used to assess the data distribution normality. For normally distributed data, one-way analysis of variance (ANOVA) followed by Tukey's post hoc test was performed to assess comparisons among groups, and Student's $t$ test was conducted to assess comparisons between two groups. For non-normally distributed data, the Kruskal–Wallis test followed by Dunn's post hoc test was used. A $p$ value greater than 0.05 means that no significant effect was observed.

## Results

### Nicotine-free e-cigarette (e-cig) induces lung tissue damage in mice

First, for evaluating the alterations in lung tissues caused by nicotine-free e-cigarette, a lung damage model was established in mice by e-cig stimulation as described. Histological analysis of lung tissues revealed significant structural alterations within the lung tissues of nicotine-free e-cigarette vapor (ECV) mice compared to control mice. Specifically, the e-cig group exhibited increased lung tissue damage, including alveolar wall thickening and inflammatory cell infiltration, indicative of emphysematous changes (Fig. 1A). Quantitative analysis of alveolar size by measuring mean linear intercept demonstrated that the alveolar size was significantly increased within the e-cig mice relative to normal controls, suggesting alveolar enlargement and destruction typically associated with emphysema (Fig. 1B). IF staining showed no obvious changes in CD31 levels and a remarkable elevation in α-SMA levels in the lung tissues of ECV mice, suggesting airway remodeling and fibrosis (Fig. 1C). IHC staining further confirmed the increase in α-SMA levels in the muscular arteries of lung tissues from the e-cig mice relative to normal controls (Fig. 1D). Quantitative analysis of the muscular artery wall area, wall thickness, wall thickness percentage (WT%), and wall area percentage (WA%) revealed significant increases in these parameters in the e-cig mice relative to normal controls, indicating vascular remodeling associated with chronic lung injury (Fig. 1E). ELISA measurements indicated elevated levels of inflammatory mediators TNF-α and IL-6, as well

(See figure on next page.)

**Fig. 1** Nicotine-free e-cigarette vapor (ECV) induces lung tissue damage in mice. A lung damage model was established in mice by ECV stimulation as described. **A** Representative images of hematoxylin and eosin (H&E) staining of histopathological changes in mouse lung tissues from control and nicotine-free ECV exposed groups. Upper: magnification = ×100; down: magnification = ×200. **B** Quantification of alveolar size in control and ECV-exposed mouse lung tissues based on H&E staining. **C** Immunofluorescence staining (IF staining) of mouse lung tissues detecting CD31 and α-SMA levels. **D** Immunohistochemical (IHC) analysis of α-SMA levels in mouse lung tissues. **E** Quantification of the muscular artery wall area, wall thickness, WA%, and WT% in mouse lung tissues based on IF and IHC staining. **F**,**G** Quantification of TNF-α, IL-6, MMP-9, MDA, and SOD levels in mouse lung tissues. ** $p < 0.01$, vs. Control

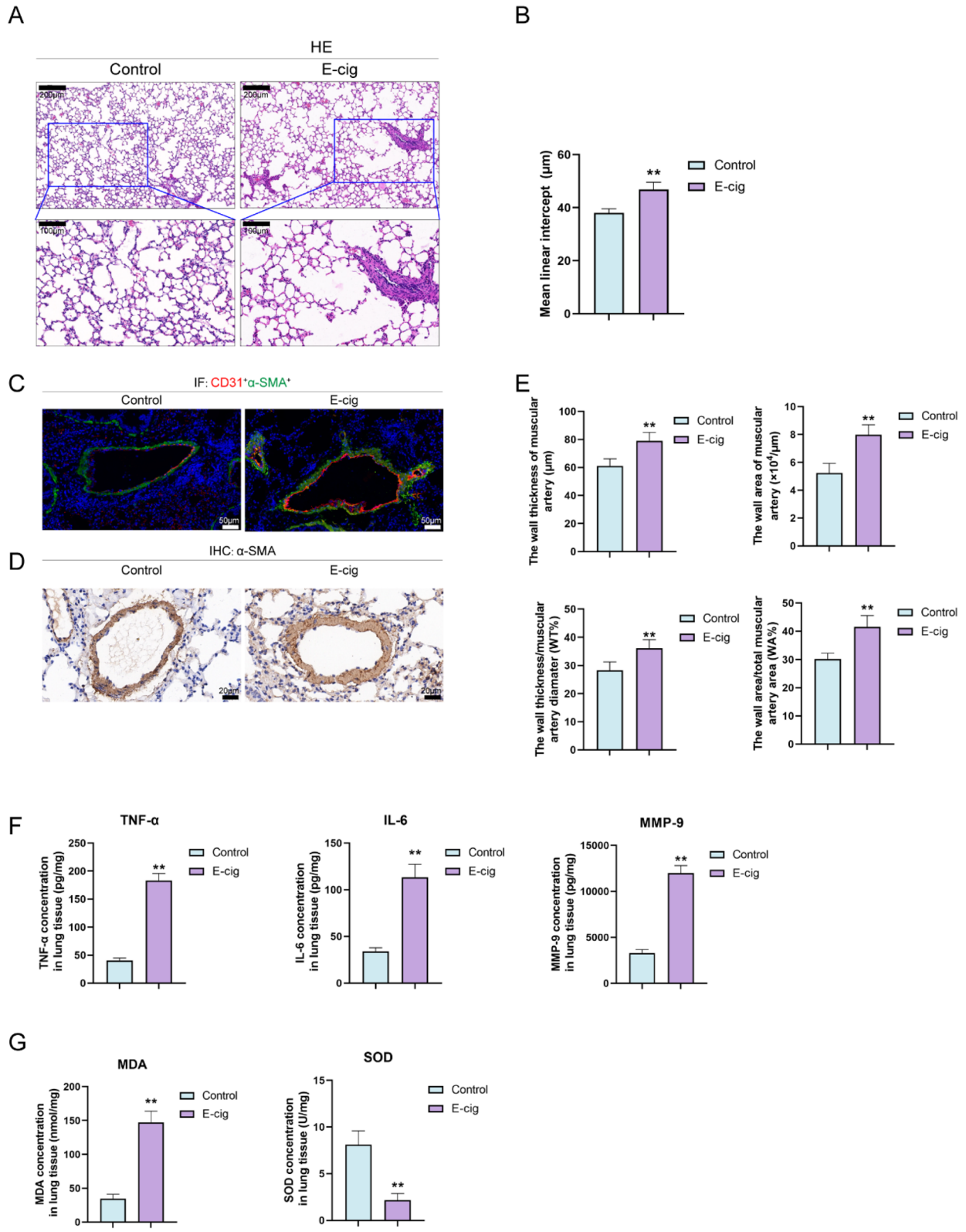


**Fig. 1** (See legend on previous page.)

as matrix metalloproteinase-9 (MMP-9) in the lung tissues of ECV mice (Fig. 1F). Additionally, markers of oxidative stress, including malondialdehyde (MDA), were significantly increased, while superoxide dismutase (SOD) levels were decreased, indicating heightened oxidative stress and impaired antioxidant defense mechanisms (Fig. 1G). These results demonstrate that exposure to ECV induces significant lung tissue damage, characterized by alveolar enlargement, vascular remodeling, and increased inflammatory and oxidative stress markers.

#### Nicotine-free e-cigarette induces glycocalyx shedding and endothelial cell damage in vivo and in vitro

MMP-9 is the marker of endothelial glycocalyx shedding through the degradation of Syndecan-1 [32]. Since elevated levels of MMP-9 were observed, and the mice also exhibited emphysema, which is associated with increased endothelial cell permeability, it was investigated whether endothelial glycocalyx damage was induced. ELISA-based quantification revealed a remarkable reduction in Syndecan-1 levels in mouse lung tissues of the e-cig mice relative to normal controls, indicating glycocalyx shedding (Fig. 2A). Conversely, the Syndecan-1 levels in BALF showed to be marked elevated within the mice, further supporting the occurrence of glycocalyx shedding (Fig. 2B). IF staining of mouse lung tissues demonstrated a notable reduction in Syndecan-1 expression and an unaltered CD31 expression within the e-cig mice relative to normal controls, indicating a disrupted endothelial glycocalyx in mice exposed to ECV (Fig. 2C).

In vitro experiments with HPMVECs demonstrated that TNF-α and IL-6 protein contents within the culture medium were increased dose-dependently following exposure to low (L-ECE), medium (M-ECE), and high (H-ECE) concentrations of e-cigarette extract (ECE) compared to control cells (Fig. 2D). Similarly, qRT-PCR indicated that TNF-α and IL-6 mRNA levels within HPMVECs exposed to ECE were significantly increased dose-dependently (Fig. 2E). ELISA revealed that MDA levels were significantly increased dose-dependently, whereas SOD levels were decreased in HPMVECs, indicating enhanced oxidative stress with higher ECE concentrations (Fig. 2F). Additionally, MMP-9 and Syndecan-1 levels in the culture medium of HPMVECs were dramatically increased dose-dependently following ECE exposure, suggesting increased glycocalyx shedding and increased extracellular matrix remodeling (Fig. 2G). IF staining of HPMVECs revealed a dose-dependent reduction in Syndecan-1 levels with increasing concentrations of ECE, indicating enhanced glycocalyx shedding by higher doses of ECE (Fig. 2H). Finally, the FITC-dextran leakage assay demonstrated that endothelial cell permeability was significantly increased dose-dependently with ECE exposure, indicating compromised endothelial barrier function (Fig. 2I). These results collectively demonstrate that nicotine-free e-cigarette induces significant glycocalyx shedding and endothelial cell damage, both in vivo and in vitro, characterized by increased inflammatory cytokines, oxidative stress, and enhanced endothelial permeability.

#### Nicotine-free e-cigarette induces mitochondrial dysfunction in endothelial cells

Since mitochondrial dysfunction is related to endothelial damage, relevant indexes were evaluated. MitoSOX Red staining revealed that mitochondrial reactive oxygen species (ROS) levels were significantly increased within HPMVECs exposed to ECE. The increase in mitochondrial ROS levels was dose-dependent, with higher concentrations of ECE (L-ECE, M-ECE, and H-ECE) leading to progressively higher ROS levels compared to the control group (Fig. 3A). JC-1 staining demonstrated alterations in mitochondrial membrane potential in HPMVECs exposed to various concentrations of ECE. Specifically, there was an elevation within JC-1 monomer (green fluorescence) intensity and a corresponding reduction within JC-1 aggregate (red fluorescence) intensity with increasing ECE concentrations, indicating a dose-dependent depolarization of the mitochondrial membrane potential (Fig. 3B). The extent of mPTP opening was also assessed. A significant decrease in fluorescence intensity was observed with increasing ECE concentrations, indicating a dose-dependent upregulation within mPTP opening.

(See figure on next page.)

**Fig. 2** Nicotine-free e-cigarette vapor induces glycocalyx shedding and endothelial cell damage in vivo and in vitro. **A** ELISA-based quantification of Syndecan-1 levels in mouse lung tissues. **B** ELISA-based quantification of Syndecan-1 levels in bronchoalveolar lavage fluid (BALF) supernatant. **C** IF staining for CD31 and Syndecan-1 in mouse lung tissues reveals the localization and relative levels of CD31 and Syndecan-1. **D** ELISA-based quantification of TNF-α and IL-6 protein levels in the culture medium of HPMVECs **E** qRT-PCR detecting the mRNA expression levels of TNF-α and IL-6 in HPMVECs. **F** Quantification of malondialdehyde (MDA) and superoxide dismutase (SOD) levels in HPMVECs. **G** ELISA-based quantification of MMP-9 and Syndecan-1 levels in the culture medium of HPMVECs. **H** IF staining for Syndecan-1 in HPMVECs. **I** FITC-dextran leakage assay to assess endothelial cell permeability in HPMVECs. * $p < 0.05$, ** $p < 0.01$, vs. Control

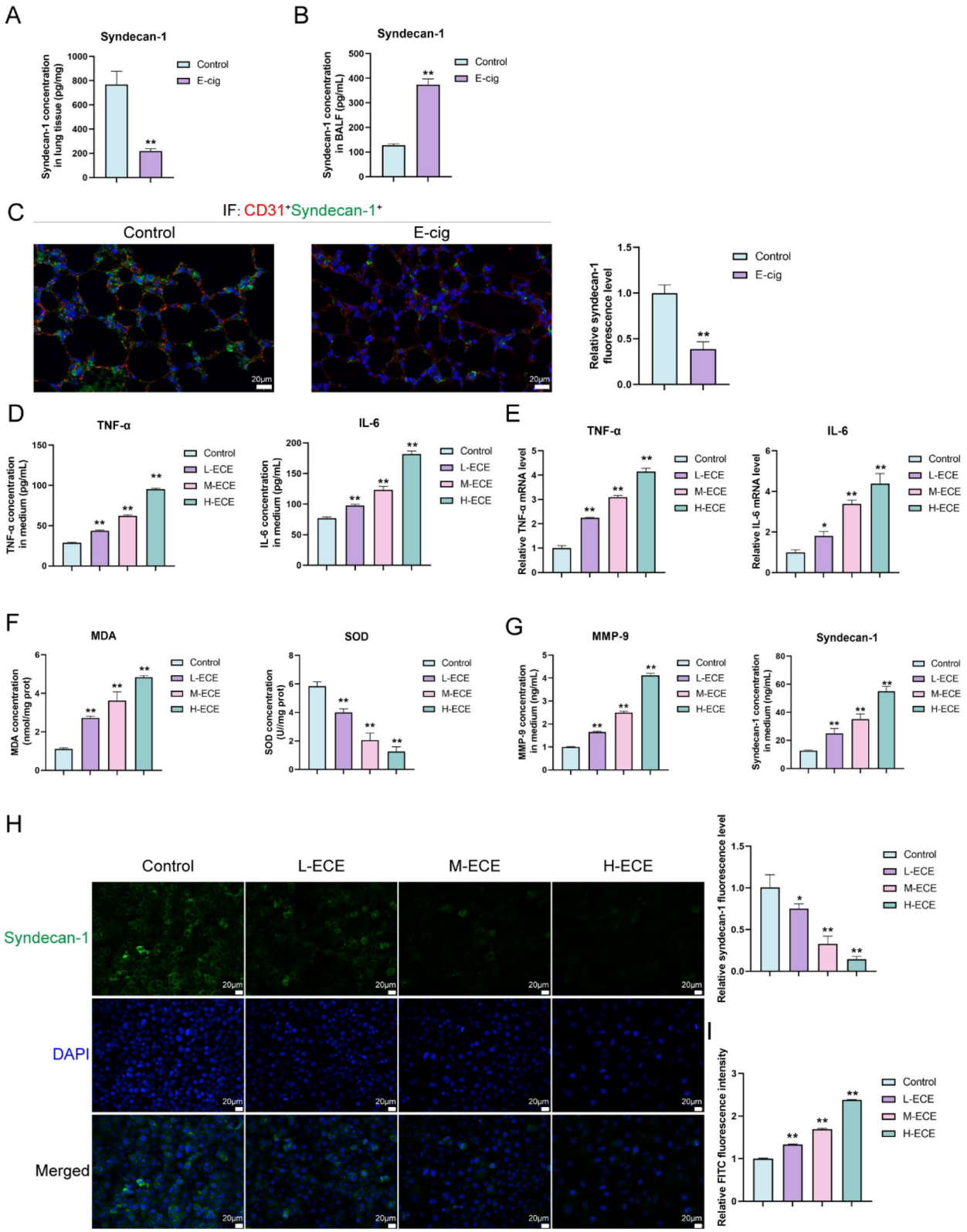


**Fig. 2** (See legend on previous page.)

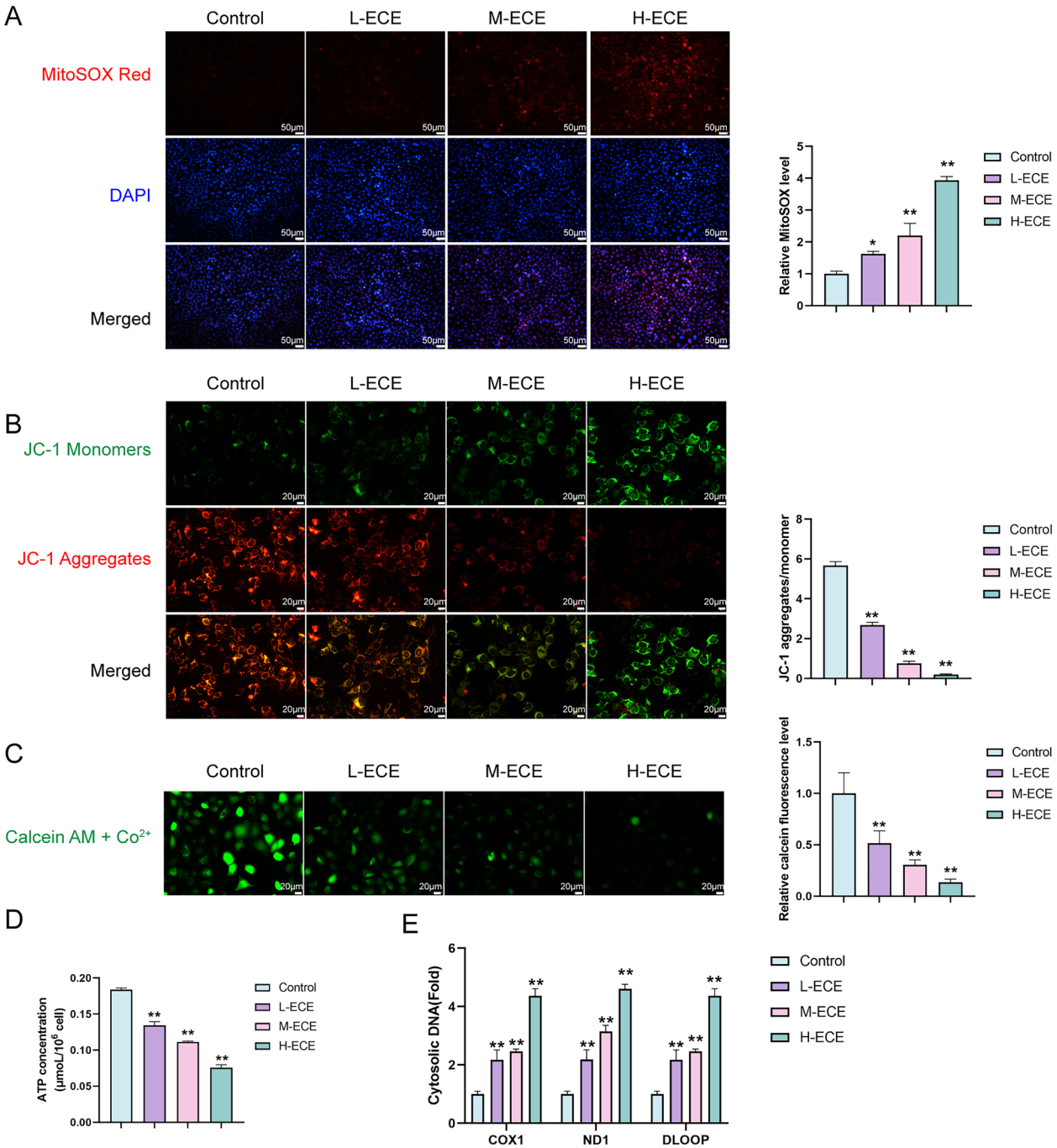


**Fig. 3** Nicotine-free e-cigarette induces mitochondrial dysfunction in endothelial cells. HPMVECs were exposed to different concentrations of nicotine-free ECE for 24 h. **A** MitoSOX Red staining was used to evaluate mitochondrial ROS levels in HPMVECs exposed to control, low, medium, and high concentrations of ECE. **B** JC-1 staining was used to assess mitochondrial membrane potential in HPMVECs. **C** The extent of mitochondrial permeability transition pore (mPTP) opening was measured using a mitochondrial permeability transition pore assay kit in HPMVECs. **D** ATP levels were measured using an ATP assay kit in HPMVECs. **E** The levels of cytosolic mitochondrial DNA (mtDNA) were quantified using real time-PCR in HPMVECs. * $p < 0.05$, ** $p < 0.01$, vs. Control

The greatest mPTP opening was found in cells exposed to the highest concentration of ECE (H-ECE) (Fig. 3C). An ATP assay kit was employed to measure ATP levels, and ATP levels showed to be significantly reduced dose-dependently within HPMVECs exposed to ECE. Higher concentrations of ECE (M-ECE and H-ECE) resulted

in the most pronounced reductions in ATP levels, indicating severe impairment of mitochondrial function (Fig. 3D). PCR analysis of mitochondrial DNA (mtDNA) levels revealed a significant increase in cytosolic mtDNA-specific genes (COX1, ND1) content in HPMVECs exposed to ECE. This increase was dose-dependent, with higher concentrations of ECE leading to higher mtDNA levels relative to normal controls (Fig. 3E). Taken together, exposure to ECE induces significant mitochondrial dysfunction in HPMVECs.

#### Inhibition of mPTP opening reverses ECE-induced mitochondrial dysfunction in endothelial cells

After confirming ECE-induced mitochondrial dysfunction in HPMVECs, the involvement of the mPTP opening was investigated. The mPTP opening extent showed to be significantly decreased via the treatment with CsA, an mPTP inhibitor, compared with the ECE group (Fig. 4A). MitoSOX Red staining showed significantly reduced ROS levels by the treatment with CsA compared to the ECE group, demonstrating the protective effect of mPTP inhibition upon mitochondrial oxidative stress induced by ECE (Fig. 4B). JC-1 staining indicated the depolarization of the mitochondrial membrane potential within endothelial cells exposed to ECE was improved by CsA treatment, as evidenced by decreased JC-1 monomers (green fluorescence) and increased JC-1 aggregates (red fluorescence) compared to the ECE group (Fig. 4C). ATP levels showed to be dramatically increased by CsA treatment relative to the ECE treated group, demonstrating the protective effect of mPTP inhibition on ATP production (Fig. 4D). Lastly, cytosolic mtDNA levels were significantly decreased within CsA-treated endothelial cells relative to the ECE treated group, indicating that CsA reduced ECE-induced mtDNA release to the cytosol (Fig. 4E). These results collectively demonstrate that inhibition of mPTP opening by CsA effectively reverses the mitochondrial dysfunction induced by ECE in endothelial cells.

#### Inhibition of mPTP opening reverses ECE-induced endothelial inflammation, glycocalyx shedding, and permeability damage

Regarding endothelial inflammation, glycocalyx shedding, and permeability alterations, TNF-α and IL-6 protein contents were examined within the culture medium of endothelial cells using ELISA; these inflammatory cytokines showed to be reduced within the ECE + CsA treatment relative to the ECE treated alone, indicating that mPTP inhibition mitigates ECE-induced inflammation (Fig. 5A). Consistently, TNF-α and IL-6 mRNA levels showed to be dramatically reduced within CsA-treated endothelial cells compared to those exposed to ECE alone (Fig. 5B). ELISA-based measurements demonstrated that CsA treatment significantly decreased MDA levels and increased SOD levels in endothelial cells exposed to ECE, indicating that mPTP inhibition by CsA reduces oxidative stress and enhances antioxidant defense mechanisms in endothelial cells (Fig. 5C). Syndecan-1 and MMP-9 levels within the culture media also showed to be remarkably reduced via CsA treatment in endothelial cells exposed to ECE, as measured by ELISA, suggesting that CsA could suppress the shedding of endothelial glycocalyx led by ECE exposure (Fig. 5D). IF staining for Syndecan-1 revealed increased expression of this glycocalyx component in endothelial cells treated with CsA compared to those exposed to ECE alone, suggesting that mPTP opening inhibition helps to maintain the integrity of the endothelial glycocalyx under ECE exposure (Fig. 5E). The FITC-dextran leakage assay demonstrated that CsA treatment significantly reduced endothelial cell permeability compared to ECE exposure alone, suggesting that mPTP inhibition by CsA could mitigate the barrier dysfunction induced by ECE in endothelial cells (Fig. 5F). These results demonstrate that inhibition of mPTP opening by CsA effectively reverses the endothelial inflammation, glycocalyx shedding, and permeability damage induced by ECE.

#### ECE promotes mPTP opening by regulating the AKT/GSK3β pathway

Regarding the underlying signaling pathway involved, the alterations in the AKT/GSK3β pathway were investigated. Immunoblotting was performed to detect phosphorylated AKT (p-AKT), total AKT, phosphorylated GSK3β (p-GSK3β, Ser9), and total GSK3β levels in endothelial cells stimulated with ECE or ECE plus SC79 (AKT agonist). Specifically, phosphorylated AKT (p-AKT) and phosphorylated GSK3β (p-GSK3β, Ser9) levels were markedly decreased within the ECE mice relative to normal controls. Treatment with SC79, an AKT agonist, partially restored p-AKT/AKT and p-GSK3β/GSK3β levels (Fig. 6A). The mPTP opening extent showed to be dramatically increased within the ECE relative to normal controls, as measured by a fluorescence assay kit. This increase in mPTP opening was partially reversed by treatment with SC79, suggesting that activation of the AKT pathway could mitigate ECE-induced mPTP opening (Fig. 6B). Consistently, a significant increase in cytosolic mtDNA content in endothelial cells of the ECE group relative to normal controls, whereas SC79 treatment partially reduced the cytosolic mtDNA levels, indicating that activation of the AKT pathway improved ECE-induced mtDNA release (Fig. 6C). These results demonstrate that ECE promotes mPTP opening through the downregulation of the AKT/GSK3β pathway.

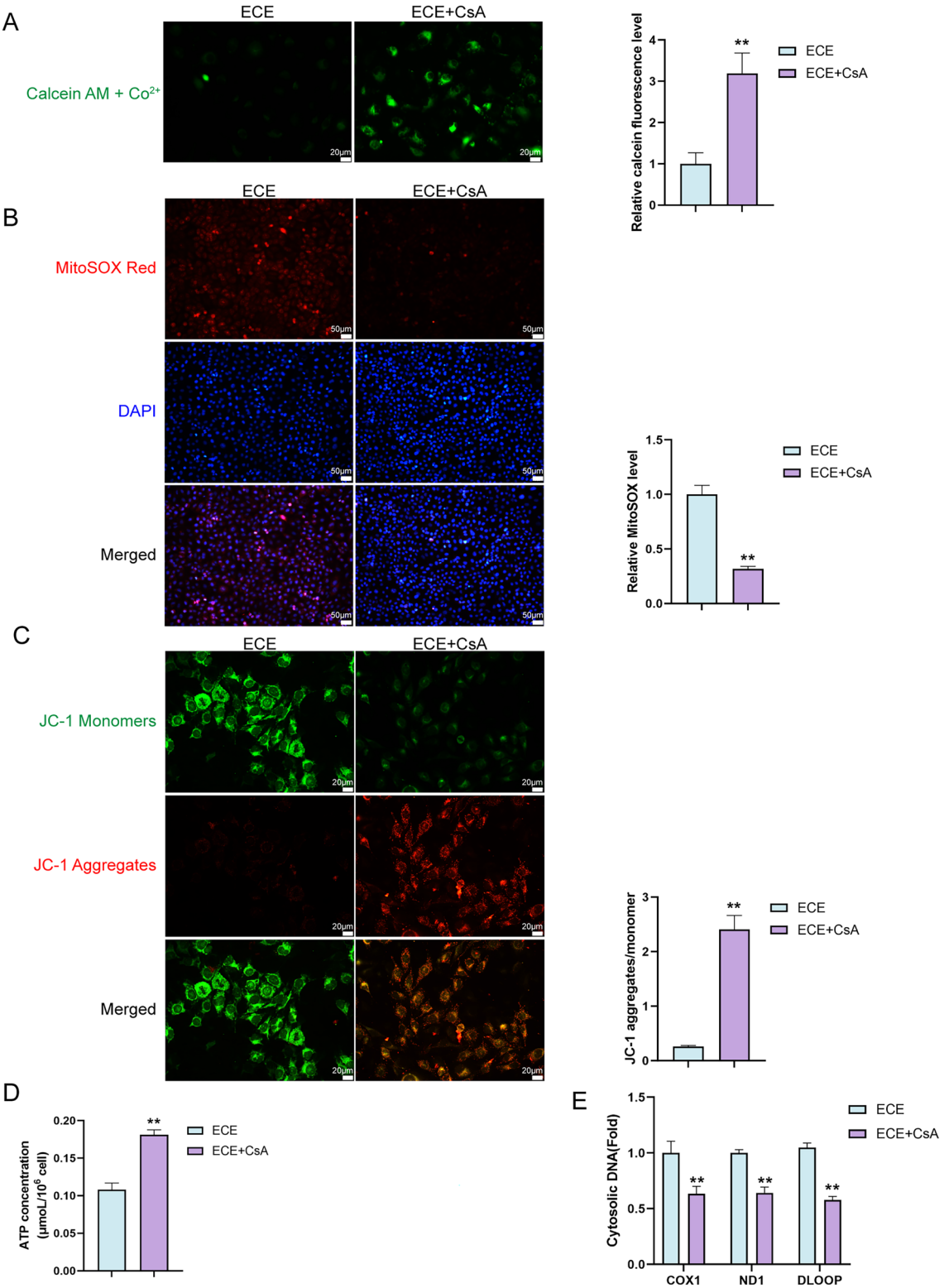


**Fig. 4** Inhibition of mPTP opening reverses ECE-induced mitochondrial dysfunction in endothelial cells. HPMVCs were exposed to the high concentration of ECE (30%) alone or co-treated with 10 μM CsA (mPTP inhibitor) for 24 h. **A** The extent of mitochondrial permeability transition pore (mPTP) opening was measured using a mitochondrial permeability transition pore assay kit in HPMVECs. **B** MitoSOX Red staining was used to evaluate mitochondrial ROS levels in HPMVECs. **C** JC-1 staining was used to assess mitochondrial membrane potential in HPMVECs. **D** ATP levels were measured using an ATP assay kit in HPMVECs. **E** Real time-PCR analysis of cytosolic mtDNA levels in HPMVECs. ** $p < 0.01$, vs. ECE

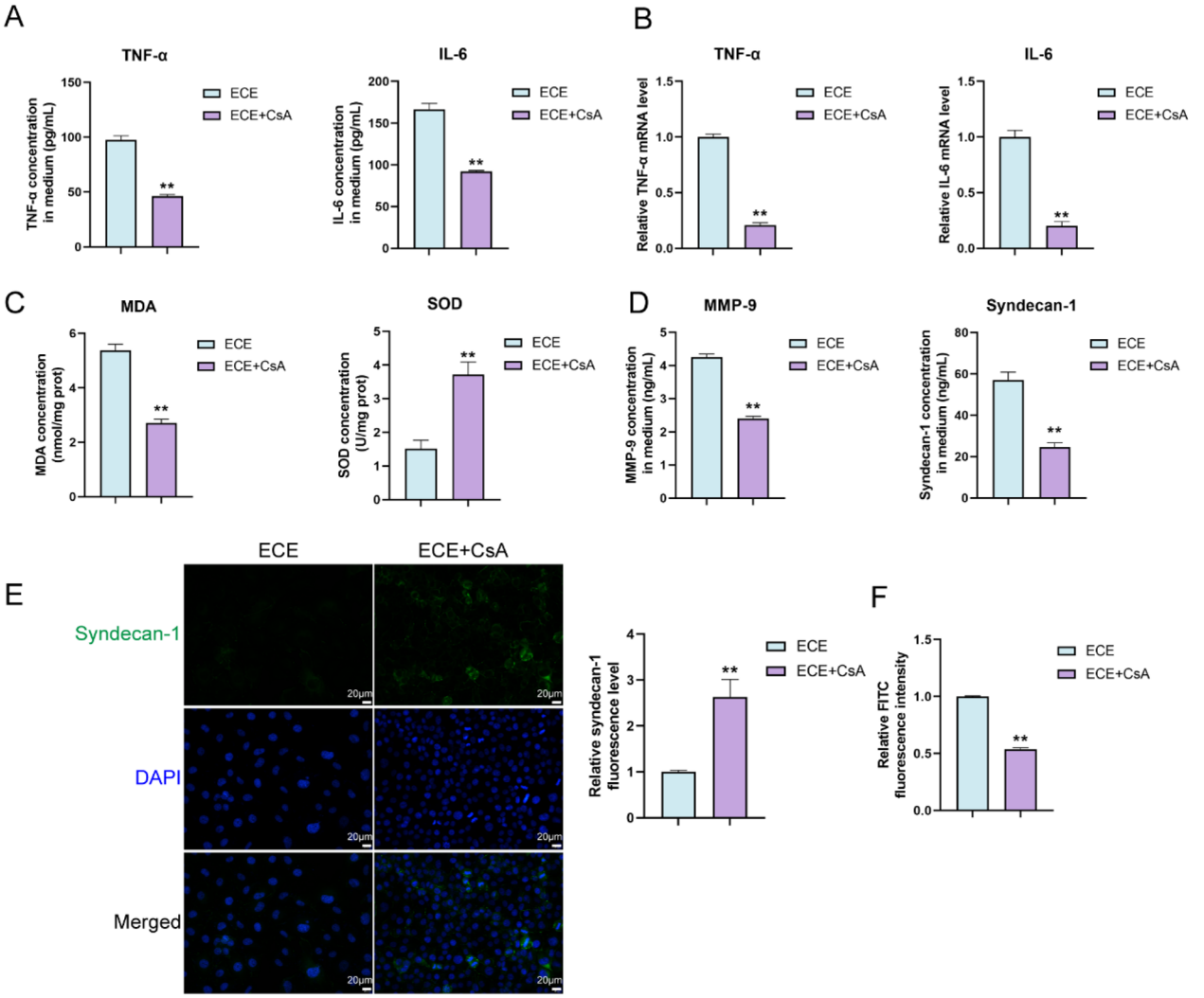


**Fig. 5** Inhibition of mPTP opening reverses ECE-induced endothelial inflammation, glycocalyx shedding, and permeability damage. HPMVECs were exposed to high concentration of ECE (30%) alone or co-treated with 10 μM CsA (mPTP inhibitor) for 24 h. **A** ELISA-based quantification of TNF-α and IL-6 protein levels in the culture medium of HPMVECs. **B** qRT-PCR detecting TNF-α and IL-6 mRNA levels in HPMVECs. **C** Quantification of MDA and SOD levels in HPMVECs. **D** ELISA-based quantification of Syndecan-1 and MMP-9 levels in the culture medium of HPMVECs. **E** IF staining for Syndecan-1 in HPMVECs. **F** FITC-dextran leakage assay to assess endothelial cell permeability in HPMVECs. ** $p < 0.01$, vs. ECE

## Discussion

This study reveals that exposure to nicotine-free ECV induces significant lung tissue damage, endothelial glycocalyx shedding, and mitochondrial dysfunction. In mice, nicotine-free ECV exposure led to alveolar enlargement, inflammatory cell infiltration, and vascular remodeling, indicative of emphysematous changes. In vitro, HPMVECs exposed to ECE showed increased levels of proinflammatory factors (TNF-α and IL-6), oxidative stress markers (MDA), and endothelial permeability, along with decreased antioxidant defenses (SOD) and glycocalyx components (Syndecan-1). Mitochondrial assessments revealed elevated mitochondrial ROS, depolarized mitochondrial membrane potential, enhanced mPTP opening, and reduced ATP production. CsA-induced mPTP opening inhibition reversed these mitochondrial dysfunctions and mitigated endothelial glycocalyx shedding and permeability damage. The study also identified the AKT/GSK3β pathway as a key regulator in these processes, where ECE downregulated p-AKT and p-GSK3β, promoting mPTP opening, which was partially reversed by the AKT agonist SC79. These findings demonstrate the adverse effects of nicotine-free e-cigarettes on lung and endothelial function, mediated through mitochondrial dysfunction and the AKT/GSK3β pathway.

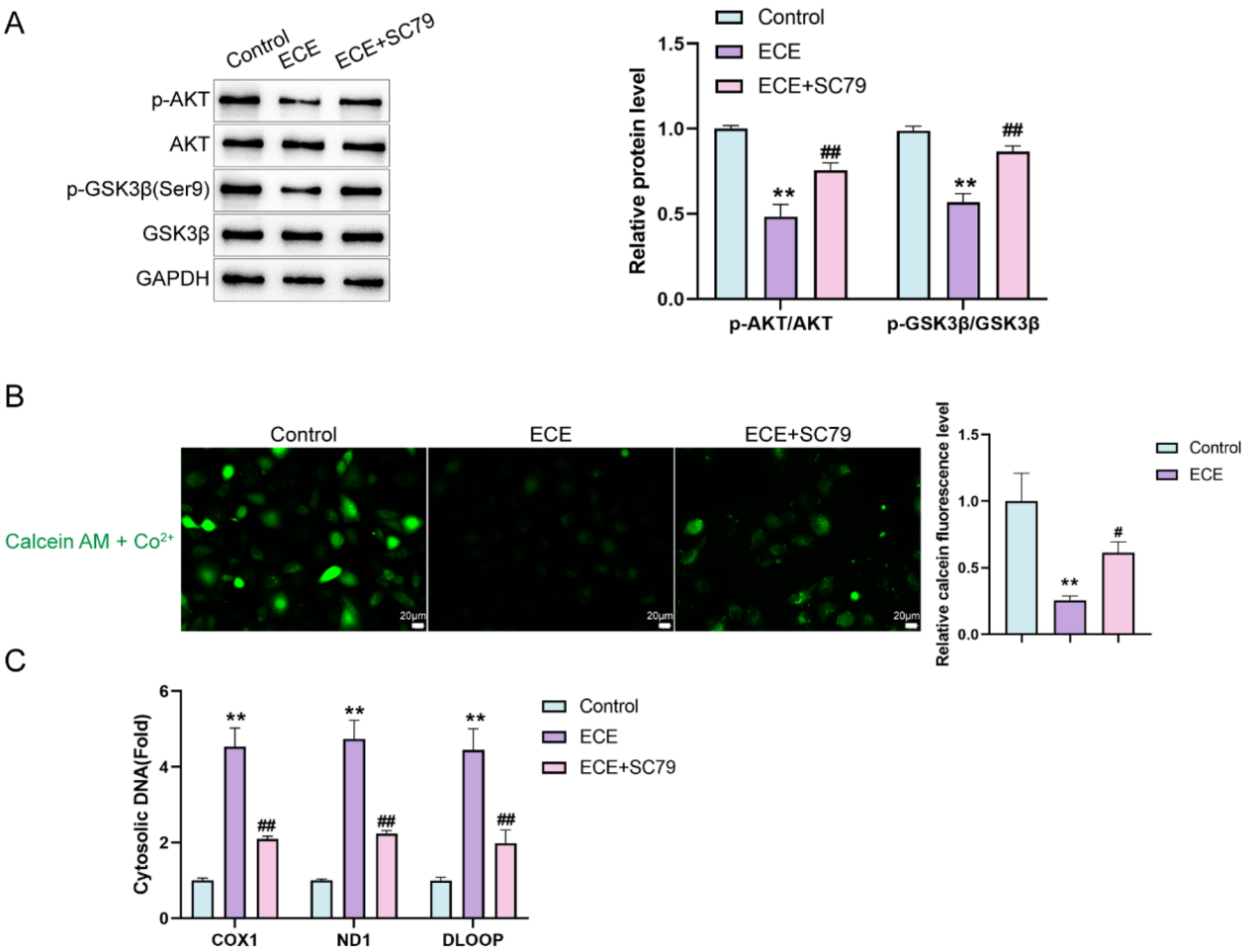


**Fig. 6** ECE promotes mPTP opening by regulating the AKT/GSK3β pathway. HPMVECs were exposed to the high concentration of ECE (30%) alone or co-treated with 4 μg/mL SC79 (AKT agonist) for 24 h. **A** Immunoblotting was performed to detect the levels of phosphorylated AKT (p-AKT), total AKT, phosphorylated GSK3β (p-GSK3β, Ser9), total GSK3β, and GAPDH in HPMVECs. **B** The extent of mPTP opening was measured using a fluorescence assay kit in HPMVECs. **C** Real time-PCR detecting cytosolic mtDNA levels in cytosol of HPMVECs. ** $p < 0.01$, vs. Control; # $p < 0.05$, ## $p < 0.01$, vs. ECE

E-cigarette or vaping product use-associated lung injury is an acute or subacute respiratory illness characterized by a spectrum of clinicopathologic findings mimicking various pulmonary diseases [33]. Although nicotine itself exhibits negative effects on pulmonary variables [34, 35], several studies revealed that the effects of e-cigarettes are nicotine-independent and associated with other components of the e-cigarette liquid or aerosol [36]. Herein, exposure to nicotine-free ECV induced significant structural damage in lung tissues, characterized by alveolar enlargement, inflammatory cell infiltration, and vascular remodeling [37], which are consistent with the emphysematous alterations commonly observed in COPD. In vitro experiments further demonstrated that HPMVEC exposure to ECE resulted in a dose-dependent upregulation in proinflammatory factors (TNF-α and IL-6), oxidative stress (MDA levels), and endothelial permeability, coupled with a decrease in antioxidant defenses (SOD levels) [38], suggesting a disrupted endothelial barrier function [39]. More importantly, elevated Syndecan-1 in BALF, and the corresponding decrease in Syndecan-1 in lung tissues were observed in ECV-stimulated mice, indicating endothelial glycocalyx shedding [32].

The pulmonary vasculature, with a total surface area of 90 $m^2$ [40], is bordered by a continuous endothelial cell monolayer coated upon the luminal side by the glycocalyx, a network of membrane-bound proteoglycans and glycoproteins linked to processes including cell–cell signaling and hemostasis [41]. Cigarette smoke has been proven to induce endothelial glycocalyx damage and emphysematous alterations within both mouse and human tissue samples [20]. In this study, HPMVEC exposure to ECE significantly impaired mitochondrial

function, indicated by increased mitochondrial ROS, depolarization of the mitochondrial membrane potential, enhanced mPTP opening, and reduced ATP production. Elevated mitochondrial ROS levels suggest oxidative stress, which could damage mitochondrial DNA, proteins, and lipids, impairing function and triggering cell death pathways [38]. In endothelial cells, increased ROS disrupts cellular signaling and promotes inflammation and vascular dysfunction, leading to compromised pulmonary blood flow and gas exchange [42], exacerbating disease symptoms. Depolarization of the mitochondrial membrane potential, essential for ATP production via the electron transport chain, indicates a loss of membrane integrity and mitochondrial dysfunction, reducing ATP synthesis and promoting mPTP opening [43]. Reduced ATP production in endothelial cells impairs functions critical for maintaining pulmonary vasculature integrity [44], contributing to tissue hypoxia and further lung damage.

Enhanced mPTP opening, a hallmark of mitochondrial distress, disrupts function and releases pro-apoptotic factors, increasing endothelial cell apoptosis and permeability, worsening vascular remodeling and inflammation [45]. Interestingly, in this study, CsA-induced mPTP opening inhibition effectively reversed ECE-elicited mitochondrial dysfunction via reducing ROS levels, increasing mitochondrial membrane potential, and improving ATP production. In lung injury, reducing ROS levels could alleviate oxidative stress, decreasing chronic inflammation and lung tissue damage [46]. By restoring mitochondrial membrane potential, CsA treatment helps maintain ATP production, ensuring endothelial functions such as maintaining barrier integrity and repairing damaged tissues [47]. CsA treatment also mitigated endothelial glycocalyx shedding and permeability alterations, suggesting that targeting mPTP could protect endothelial cells from e-cigarette-induced damage, preserving the glycocalyx and maintaining endothelial barrier function, which is crucial in preventing excessive vascular permeability and inflammation in lung injury.

As previously reported, the Akt-GSK3β-mPTP signaling could regulate the mitochondrial dysfunction, thereby promoting glucose oxidative stress-induced apoptosis of odontoblasts [26]; it also modulates mitochondrial dysfunction linked to OPA1 cleavage, which might improve the apoptosis of osteoblasts induced by oxidative stress [27]. In this study, HPMVEC exposure to ECE downregulated p-AKT and p-GSK3β, promoting mPTP opening and suggesting that disruption of this signaling exerts a pivotal effect on mitochondrial impairment and subsequent endothelial dysfunction. SC79-induced AKT signaling activation partially reversed these effects, highlighting the potential of targeting this pathway to mitigate mitochondrial and endothelial damage caused by ECE.

This study has several limitations that must be considered when interpreting the findings. One major limitation is that the research was conducted solely in mice and cell models, which may not fully represent the complexity of human systems. Therefore, the findings cannot be directly translated to humans without further validation. Additionally, our laboratory lacks the appropriate equipment to assess endothelial cell permeability in real time. Furthermore, the study also focused on short-term effects, and the long-term impact of the intervention remains unclear. To address these limitations, future research should focus on validating these findings in more complex systems, such as monkeys that better mimic human conditions, and ultimately, clinical trials in humans. Incorporating Electric Cell-Substrate Impedance Sensing (ECIS) system for endothelial permeability analysis would also provide deeper insights into the real-time effects on endothelial function. Additionally, future studies should explore other signaling pathways that may interact with those identified in this study.

In conclusion, this study demonstrates that exposure to nicotine-free e-cigarettes induces significant lung tissue damage, endothelial glycocalyx shedding, and mitochondrial dysfunction, mediated through the disruption of the AKT/GSK3β-mPTP pathway, highlighting the potential therapeutic benefits of targeting this pathway to mitigate the adverse effects of e-cigarette exposure on lung and endothelial function, particularly in the context of lung injury.

## Supplementary Information

The online version contains supplementary material available at https://doi.org/10.1186/s12931-025-03155-3.

**Additional file 1.**

**Additional file 2.**

**Acknowledgements**
None.

**Author contributions**
Ziyu Dai, Qiong Chen and Jingyi Sun contributed to experimental design and supervising the whole experimental process; Ziyu Dai, Bin Xie and Chen Jiang were involved in the experimental conducting; Yun Peng and Jianing Lin contributed to the data analysis and manuscript preparation. All the authors read, revised and approved the final manuscript.

**Funding**
This study was supported by the National Natural Science Foundation of China (No. 82370055), the Fundamental Research Funds for the Central Universities of Central South University (2024ZZTS0171), the Hunan Province Graduate Research and Innovation Project Fund (CX20240326), and the Health Research Project of Hunan Provincial Health Commission (202214054499).

**Availability of data and materials**
No datasets were generated or analysed during the current study. The authors confirm that the data supporting the findings of this study are available within the article.

## Declarations

**Ethics approval**
The guidelines for the care and use of animals were approved by the Medicine Animal Welfare Committee of Xiangya Hospital.

**Consent for publication**
Not applicable.

**Competing interests**
The authors declare no competing interests.

**Author details**
[1]Department of Geriatrics, Respiratory Medicine, Xiangya Hospital, Central South University, Changsha 410008, Hunan, China. [2]National Clinical Research Center for Geriatric Disorders, Xiangya Hospital, Central South University, Changsha 410008, Hunan, China.

Received: 11 November 2024 Accepted: 13 February 2025
Published online: 01 March 2025

**References**

1. Flor LS, Anderson JA, Ahmad N, Aravkin A, Carr S, Dai X, Gil GF, Hay SI, Malloy MJ, McLaughlin SA, et al. Health effects associated with exposure to secondhand smoke: a burden of proof study. Nat Med. 2024;30:149–67.
2. Maddatu J, Anderson-Baucum E, Evans-Molina C. Smoking and the risk of type 2 diabetes. Transl Res. 2017;184:101–7.
3. Lugg ST, Scott A, Parekh D, Naidu B, Thickett DR. Cigarette smoke exposure and alveolar macrophages: mechanisms for lung disease. Thorax. 2022;77:94–101.
4. Ishida M, Sakai C, Kobayashi Y, Ishida T. Cigarette smoking and atherosclerotic cardiovascular disease. J Atheroscler Thromb. 2024;31:189–200.
5. Gibbs K, Collaco JM, McGrath-Morrow SA. Impact of tobacco smoke and nicotine exposure on lung development. Chest. 2016;149:552–61.
6. Tarran R, Barr RG, Benowitz NL, Bhatnagar A, Chu HW, Dalton P, Doerschuk CM, Drummond MB, Gold DR, Goniewicz ML, et al. E-cigarettes and cardiopulmonary health. Function. 2021;2:zqab004.
7. Rowell TR, Tarran R. Will chronic e-cigarette use cause lung disease? Am J Physiol Lung Cell Mol Physiol. 2015;309:L1398–409.
8. Glantz SA, Bareham DW. E-cigarettes: use, effects on smoking, risks, and policy implications. Annu Rev Public Health. 2018;39:215–35.
9. Park JA, Crotty Alexander LE, Christiani DC. Vaping and lung inflammation and injury. Annu Rev Physiol. 2022;84:611–29.
10. Bozier J, Rutting S, Xenaki D, Peters M, Adcock I, Oliver BG. Heightened response to e-cigarettes in COPD. ERJ Open Res. 2019;5: 00192-2018.
11. Li CL, Liu JF, Liu SF. Mitochondrial dysfunction in chronic obstructive pulmonary disease: unraveling the molecular nexus. Biomedicines. 2024;12:814.
12. Pokharel MD, Garcia-Flores A, Marciano D, Franco MC, Fineman JR, Aggarwal S, Wang T, Black SM. Mitochondrial network dynamics in pulmonary disease: bridging the gap between inflammation, oxidative stress, and bioenergetics. Redox Biol. 2024;70: 103049.
13. Bernardi P, Gerle C, Halestrap AP, Jonas EA, Karch J, Mnatsakanyan N, Pavlov E, Sheu SS, Soukas AA. Identity, structure, and function of the mitochondrial permeability transition pore: controversies, consensus, recent advances, and future directions. Cell Death Differ. 2023;30:1869–85.
14. Robichaux DJ, Harata M, Murphy E, Karch J. Mitochondrial permeability transition pore-dependent necrosis. J Mol Cell Cardiol. 2023;174:47–55.
15. Shen Y, Chen L, Chen J, Qin J, Wang T, Wen F. Mitochondrial damage-associated molecular patterns in chronic obstructive pulmonary disease: pathogenetic mechanism and therapeutic target. J Transl Int Med. 2023;11:330–40.
16. Foote CA, Soares RN, Ramirez-Perez FI, Ghiarone T, Aroor A, Manrique-Acevedo C, Padilla J, Martinez-Lemus L. Endothelial glycocalyx. Compr Physiol. 2022;12:3781–811.
17. Bar A, Targosz-Korecka M, Suraj J, Proniewski B, Jasztal A, Marczyk B, Sternak M, Przybylo M, Kurpinska A, Walczak M, et al. Degradation of glycocalyx and multiple manifestations of endothelial dysfunction coincide in the early phase of endothelial dysfunction before atherosclerotic plaque development in apolipoprotein E/low-density lipoprotein receptor-deficient mice. J Am Heart Assoc. 2019;8: e011171.
18. Abassi Z, Armaly Z, Heyman SN. Glycocalyx degradation in ischemia-reperfusion injury. Am J Pathol. 2020;190:752–67.
19. Rizzo AN, Dudek SM. Endothelial glycocalyx repair: building a wall to protect the lung during sepsis. Am J Respir Cell Mol Biol. 2017;56:687–8.
20. Jiang T, Hu W, Zhang S, Ren C, Lin S, Zhou Z, Wu H, Yin J, Tan L. Fibroblast growth factor 10 attenuates chronic obstructive pulmonary disease by protecting against glycocalyx impairment and endothelial apoptosis. Respir Res. 2022;23:269.
21. Strutynska NA, Balatskyi VV, Strutynskyi RB, Goshovska YV, Mys LA, Luchkova AY, Denysova MV, Korkach YP, Strutynskyi VR, Piven OO, et al. Pyridoxal-5-phosphate mitigates age-related metabolic imbalances in the rat heart through the $H_2S$/AKT/GSK3β signaling axis. Mitochondrion. 2025;81: 102001.
22. Kan H, Wang P, Yang Y, Jia H, Liu A, Wang M, Ouyang C, Yang X. Apigenin inhibits proliferation and differentiation of cardiac fibroblasts through AKT/GSK3β signaling pathway. J Ethnopharmacol. 2024;334: 118518.
23. Guo Z, Zhang J, Li M, Xing Z, Li X, Qing J, Zhang Y, Zhu L, Qi M, Zou X. Mechanism of action of quercetin in regulating cellular autophagy in multiple organs of Goto-Kakizaki rats through the PI3K/Akt/mTOR pathway. Front Med. 2024;11:1442071.
24. Liu M, Huang X, Tian Y, Yan X, Wang F, Chen J, Zhang Q, Zhang Q, Yuan X. Phosphorylated GSK-3β protects stress-induced apoptosis of myoblasts via the PI3K/Akt signaling pathway. Mol Med Rep. 2020;22:317–27.
25. Jiang B, Guan Y, Shen HJ, Zhang LH, Jiang JX, Dong XW, Shen HH, Xie QM. Akt/PKB signaling regulates cigarette smoke-induced pulmonary epithelial-mesenchymal transition. Lung Cancer. 2018;122:44–53.
26. Wu D, Yan L, Zheng C, Ren X, Pan Y, Huang S, Pan L, Li Z. Akt-GSK3β-mPTP pathway regulates the mitochondrial dysfunction contributing to odontoblasts apoptosis induced by glucose oxidative stress. Cell Death Discov. 2022;8:168.
27. Cai WJ, Chen Y, Shi LX, Cheng HR, Banda I, Ji YH, Wang YT, Li XM, Mao YX, Zhang DF, et al. AKT-GSK3β signaling pathway regulates mitochondrial dysfunction-associated OPA1 cleavage contributing to osteoblast apoptosis: preventative effects of hydroxytyrosol. Oxid Med Cell Longev. 2019;2019:4101738.
28. Tang MS, Wu XR, Lee HW, Xia Y, Deng FM, Moreira AL, Chen LC, Huang WC, Lepor H. Electronic-cigarette smoke induces lung adenocarcinoma and bladder urothelial hyperplasia in mice. Proc Natl Acad Sci USA. 2019;116:21727–31.
29. Fung NH, Nguyen QA, Owczarek C, Wilson N, Doomun NE, De Souza D, Quinn K, Selemidis S, McQualter J, Vlahos R, et al. Early-life house dust mite aeroallergen exposure augments cigarette smoke-induced myeloid inflammation and emphysema in mice. Respir Res. 2024;25:161.
30. Roxlau ET, Pak O, Hadzic S, Garcia-Castro CF, Gredic M, Wu CY, Schäffer J, Selvakumar B, Pichl A, Spiegelberg D, et al. Nicotine promotes e-cigarette vapour-induced lung inflammation and structural alterations. Eur Respir J. 2023;61:2200951.
31. Liu Z, Zhang Y, Youn JY, Zhang Y, Makino A, Yuan JX, Cai H. Flavored and nicotine-containing e-cigarettes induce impaired angiogenesis and diabetic wound healing via increased endothelial oxidative stress and reduced NO bioavailability. Antioxidants. 2022;11:904.
32. Zhang D, Zhang JT, Pan Y, Liu XF, Xu JW, Cui WJ, Qiao XR, Dong L. Syndecan-1 shedding by matrix metalloproteinase-9 signaling regulates alveolar epithelial tight junction in lipopolysaccharide-induced early acute lung injury. J Inflamm Res. 2021;14:5801–16.
33. Zulfiqar H, Sankari A, Rahman O. Vaping-associated pulmonary injury. In: StatPearls. Treasure Island: StatPearls Publishing; 2024.

34. Ahmad S, Zafar I, Mariappan N, Husain M, Wei CC, Vetal N, Eltoum IA, Ahmad A. Acute pulmonary effects of aerosolized nicotine. Am J Physiol Lung Cell Mol Physiol. 2019;316:L94–104.
35. Behar RZ, Wang Y, Talbot P. Comparing the cytotoxicity of electronic cigarette fluids, aerosols and solvents. Tob Control. 2018;27:325–33.
36. Marques P, Piqueras L, Sanz MJ. An updated overview of e-cigarette impact on human health. Respir Res. 2021;22:151.
37. Sohal SS, Ward C, Danial W, Wood-Baker R, Walters EH. Recent advances in understanding inflammation and remodeling in the airways in chronic obstructive pulmonary disease. Expert Rev Respir Med. 2013;7:275–88.
38. Barnes PJ. Oxidative stress-based therapeutics in COPD. Redox Biol. 2020;33: 101544.
39. Theodorakopoulou MP, Alexandrou ME, Bakaloudi DR, Pitsiou G, Stanopoulos I, Kontakiotis T, Boutou AK. Endothelial dysfunction in COPD: a systematic review and meta-analysis of studies using different functional assessment methods. ERJ Open Res. 2021;7: 00983-2020.
40. Goldenberg NM, Kuebler WM. Endothelial cell regulation of pulmonary vascular tone, inflammation, and coagulation. Compr Physiol. 2015;5:531–59.
41. Suzuki A, Tomita H, Okada H. Form follows function: the endothelial glycocalyx. Transl Res. 2022;247:158–67.
42. Bernardo I, Bozinovski S, Vlahos R. Targeting oxidant-dependent mechanisms for the treatment of COPD and its comorbidities. Pharmacol Ther. 2015;155:60–79.
43. Webster KA. Mitochondrial membrane permeabilization and cell death during myocardial infarction: roles of calcium and reactive oxygen species. Future Cardiol. 2012;8:863–84.
44. Stevens RP, Paudel SS, Johnson SC, Stevens T, Lee JY. Endothelial metabolism in pulmonary vascular homeostasis and acute respiratory distress syndrome. Am J Physiol Lung Cell Mol Physiol. 2021;321:L358–76.
45. Lerner CA, Sundar IK, Rahman I. Mitochondrial redox system, dynamics, and dysfunction in lung inflammaging and COPD. Int J Biochem Cell Biol. 2016;81:294–306.
46. Bezerra FS, Lanzetti M, Nesi RT, Nagato AC, Silva CPE, Kennedy-Feitosa E, Melo AC, Cattani-Cavalieri I, Porto LC, Valenca SS. Oxidative stress and inflammation in acute and chronic lung injuries. Antioxidants. 2023;12:548.
47. Zhao Z, Zhu P, Lou Y, Hou R, Sun H, Du Y, Xu G. Receptor-interacting protein kinase 3-mediated modulation of endothelial cell necroptosis and mitochondrial dysfunction through AMPK/Drp1 signaling pathway: insights into the pathophysiological mechanisms of lipopolysaccharide-induced acute lung injury. Int J Med Sci. 2025;22:71–86.


## Publisher's Note